Available online at www.sciencedirect.com

ScienceDirect

Procedia CIRP 94 (2020) 936–941

www.elsevier.com/locate/procedia

11th CIRP Conference on Photonic Technologies [LANE 2020] on September 7-10, 2020

Ultrashort pulse laser micro polishing of steel – Investigation of the melt pool depth

M. Osbild[a,*], A. Brenner[a], L. Röther[b], J. Finger[a]

[a]*Fraunhofer-Institute for Laser Technology (ILT), Steinbachstr. 15, 52074 Aachen, Germany*
[b]*Chair for Laser Technology (LLT), RWTH Aachen, Steinbachstr. 15, 52074 Aachen, Germany*

* Corresponding author. Tel.: +49 241-8906-325; fax: +49-241-8906-121. *E-mail address:* martin.osbild@ilt.fraunhofer.de

Abstract

For the most demanding applications in mold and tool manufacturing, ultrashort pulsed laser structured surfaces sometimes do not meet the requirements for surface roughness. A subsequent polishing step in the same machine with the same beam source offers a time and cost effective solution. The novel approach of ultrashort pulse laser polishing with a pulse duration of τ = 10 ps is investigated experimentally and theoretically in the present study. It is shown that a low micro roughness is achieved with a melt pool depth between 1 and 3 µm in hot-working steel 1.2738, which allows a polishing process for surface structures with small and fine geometry features without influencing the structure itself.

Keywords: Ultrashort pulse laser; polishing; burst; melt pool depth; surface quality; roughness

1. Introduction

Ultrashort pulse lasers have proven their advantage in high precision structuring with minimal thermal impact on the surrounding material in many applications. However, if an excellent surface quality is demanded (e.g. in lighting applications), the surface roughness has to be further decreased. Since the structure sizes are in the range of a few microns, manual polishing is too challenging for the subsequent polishing step. Machine-supported polishing processes also fail due to the sometimes complex and small structure sizes [1].

To meet customer requirements, one approach is to apply an additional laser polishing process with long pulse durations in a separate machine [2,3]. Shortening this process chain by using ultrashort pulse laser polishing in the same machine as the ablation process is desirable in terms of time and cost [4,5].

BRENNER et al. have shown that the ultrashort pulse laser polishing process is feasible but very sensitive [6]. A controlled heat accumulation is crucial to hit the narrow process window. A molten phase is needed to smooth the roughness peaks and polish the workpiece. The process dominating parameters are the applied fluence and the number of pulses per burst.

According to WISSENBACH et al. the melt pool depth determines what maximum roughness depth is possible to smooth [7]. Therefore it is important to know the melt pool depth for a better understanding of the ultrashort pulse laser polishing process. Due to its novelty, the influence of the process parameters on the melt pool depth and the influence of the melt pool depth on the roughness have not been investigated yet. These topics and furthermore the microstructure change in the surface layer as a result of the polishing process are addressed in the present study.

10.1016/j.procir.2020.09.094

2. Experimental setup

The specimens used in the experimental investigations are hot-working steel blanks (1.2738) with a thickness of 10 mm to provide dimensional stability. The blanks have a ground initial surface with an average surface roughness of about S_a = 0.3 µm. The grinding grooves are straight and non-directional. The threshold fluence of this material is F_{thr} = 0.12 J/cm² for a single pulse according to the logarithmic relationship between the single pulse peak fluence F_0 and power specific volume ablation rate $\dot{V}_{ablation}/P_{av}$ [8–10]. However, it is questionable to transfer this value for burst processes due to heat accumulation.

The experiments are carried out on the 5-axis machining system AGIE CHARMILLES LASER P 1000 U from GF MACHINING SOLUTIONS. The machining system is equipped with an infrared (λ_L = 1064 nm) ultrashort pulse laser beam source from EDGEWAVE. It provides a maximum average power of P_{av} = 50 W and a pulse duration of τ = 10 ps. The adjustable pulse repetition frequency ranges from f_{rep} = 250 kHz to 2 MHz. The seeder frequency is f_{seed} = 49.8 MHz which also determines the temporal distance between the consecutive pulses within a pulse train while burst processing. The laser is focused on the specimen surface with a focal length of f = 125 mm. The focus diameter (1/e²) measured with a camera based beam profiler is about $2w_0$ = 37 µm.

Square fields with an edge length of 5 mm are polished on the steel blanks with varying process parameters. Preliminary tests have shown that smaller fields can lead to heat accumulation between two subsequent repetitions, depending on the process parameters used. However, this form of heat accumulation should be excluded in favor of better reproducibility and comparability. The scanning of the field is performed in a straight and bidirectional way with the galvanometer scanner INTELLISCAN III 14 from SCANLAB. The scanning direction is rotated by an angle of 90° after each repetition, so that the scan vectors of subsequent layers are perpendicular to each other.

The selection of parameters represents an excerpt from the broad parameter study by BRENNER et al. [6]. An overview of the used parameter settings is given in Table 1.

Table 1. Overview of the parameter settings used in this experimental work.

Pulse per burst PpB [-]	14–20
Fluence F_0 [J/cm²]	0.065–0.165
Repetition frequency f_{rep} [kHz]	2000
Scan speed v_{scan} [m/s]	4.5
Line distance LD [µm]	4.5
Number of repetitions N [-]	2–128
Spot diameter $2w_0$ [µm]	37
Initial surface roughness S_a [µm]	0.32

3. Measuring methods

3.1. Surface roughness

The main goal of laser polishing is to achieve a low roughness. In order to validate this purpose, the laser scanning microscope (LSM) VK-9700 from KEYENCE is used for the topography measurement. The images for measuring the roughness have a size of 270 x 202 µm². Three neighboring fields are measured at once to estimate the statistical variation of the roughness of one polished square field.

The quality of laser machined surfaces is quantified by the surface roughness S_a (µm) that is calculated from an optical surface topography measurement and can be seen as an extension of the more common R_a-value in one dimension [11]:

$$S_a = \frac{1}{A}\iint_A |z(x,y)|\,dx\,dy \quad (1)$$

The raw LSM images are post-processed with the software MOUNTAINSMAP from DIGITAL SURF that corrects the tilt and filters the surface roughness S_a by spatial wavelengths λ. The S_a-spectrum is divided into three spatial wavelength ranges: micro (<10 µm), meso (10–80 µm) and macro roughness (80–320 µm) [12]. Previous evaluations have shown that a look at the general roughness without the division into spatial wavelengths does not lead to useful results, because the grinding grooves, which are mainly responsible for the macro roughness, overshadow the other roughness components. Furthermore, in the case of periodically ablated surface structures, for instance, it is not intended that the corresponding waviness is eliminated. It is known that short pulse durations tend to polish only within short spatial wavelengths anyway [13]. The conclusion is that the focus of this work lies on the influences on the micro and meso roughness, which is also the roughness range responsible for a glossy surface [12]. The roughness components with spatial wavelengths λ below 1.6 µm are cut off due to the resolution limit of the LSM. The error bars of the S_a-values represent the standard deviation from three measurements. The roughness of the initial surface filtered by spatial wavelengths is given in table 2.

Table 2. Roughness of the initial surface filtered by spatial wavelengths.

Initial surface micro roughness S_a [µm] ($1.6 < \lambda < 10$ µm)	0.12
Initial surface meso roughness S_a [µm] ($10 < \lambda < 80$ µm)	0.15

3.2. Melt pool depth

A small melt pool depth is required when the geometry of very fine structures must not be influenced by the polishing process. To measure the melt pool depth, the specimens are separated with a cut-off wheel perpendicular to the last scan direction. The halves are embedded in a cold-curing polymer for further preparation. The specimen are then mechanically ground in stages from coarse to fine and finally polished. The polished cross sections are etched in Nital (3% nitric acid, 97% ethanol) for 45 seconds to increase the contrast between the basic structure and the melting layer. The melt pool depth is then determined using the average of the layer thickness through 30 points at regular intervals perpendicular to the specimen surface. The error bars of the melt pool depths z_m represent the whole range of detected values.

3.3. Microstructure of the surface layer

The microstructure of the melting layer is examined using electron backscatter diffraction (EBSD). EBSD is an analytical method of scanning electron microscopy, which delivers morphological (grain size) and crystallographic (grain orientation and phase) information about the microstructure of the melting layer.

For EBSD analysis, a special sample preparation is required. To be able to examine the surface layer, the samples are coated with gold in a sputter coater to ensure surface conductivity. Subsequently, the samples are galvanically nickel-plated in an electrolysis bath to minimize edge rounding during the cross section preparation. The resulting nickel layer is about 20 µm wide. The samples are then hot-embedded in a conductive embedding material, ground and polished in stages. The final polishing is carried out with colloidal SiO_2 with a grain size of 50 nm). The polishing is largely done manually.

The field-emission scanning electron microscope JSM-7000F of the manufacturer JEOL is used. The acceleration voltage is 15 kV, the sample current 30 nA. The analysis area measures 100 x 100 µm². The measurement data are post-processed with the software ORIENTATION IMAGING MICROSCOPY (OIM) DATA COLLECTION from EDAX and evaluated with the associated software OIM ANALYSIS.

4. Simulation model

The simulation model used in this thesis is the same as the one used in the work of BRENNER et al [6]. In this section, the relevant physical backgrounds are summarized. The following equation describes the predominant energy balance of the energy absorbed by the work piece:

$$A \cdot E_P = E_{ablation} + E_{\text{heat}} \quad \text{with } E_{heat} = \eta_{res} \cdot E_P \tag{2}$$

For ultrashort laser ablation a certain amount of the laser pulse energy E_P incident on the sample surface does not contribute to the ablation process and is deposited as residual heat (E_{heat}) in the material. The percentage of this residual heat from the incident pulse energy E_P is represented by the coefficient η_{res}. For the process of ultrashort pulse polishing with single pulse fluences below the ablation threshold, the energy contributing to ablation ($E_{ablation}$) is assumed to be zero, so that the energy balance reads as follows:

$$A \cdot E_P = \overbrace{E_{ablation}}^{0} + \eta_{res} \cdot E_P \Leftrightarrow A = \eta_{res} \tag{3}$$

Considering the high pulse and line overlap, an incident pulse barely hits the initial ground surface with its absorptance of $A = 0.42$. Therefore, the absorptance is assumed to be $A = 0.44$, which equals the average of the ex situ measured absorptance of ultrashort pulse polished surfaces. Assuming that the spatial laser intensity distribution follows a Gaussian beam profile and represents a surface heat source, the temperature raise at $t = 0$ at the location $(x_0, y_0, 0)$ can be calculated by [14]

$$T^{s.p.}_{x_0,y_0}(x,y,z,t) = \frac{2\eta_{res} \cdot E_P}{\pi\rho c \cdot \sqrt{\pi\kappa t}(8\kappa t + w_0^2)} \cdot \exp\left[\frac{(x-x_0)^2 + \left(y-y_0\right)^2}{4\kappa t} \cdot \left(\frac{w_0^2}{8\kappa t + w_0^2} - 1\right)\right] \cdot \exp\left[-\frac{z^2}{4\kappa t}\right] \tag{4}$$

with laser pulse energy E_P, focus radius w_0, density ρ, specific heat capacity c and thermal diffusivity κ.

For a burst with n pulses and a scan speed v_{scan} along the x-axis the temperature distribution follows [15]

$$T^{b}_{x_0,0}(x,y,z,t) = \sum_{i=0}^{n-1} T^{s.p.}_{x_i,0}(x,y,z,t_i) \tag{5}$$

Table 3 gives an overview about the material properties of hot-working steel 1.2738 at a temperature of 973.15 K that are used for the analytic simulation model. Taking the melting enthalpy into account, the melting temperature for 1.2738 is set to 2139.15 K.

Table 3. Material properties of hot-working steel 1.2738 at a temperature of 973.15 K used for the simulation of the temperature distribution during ultrashort pulsed polishing processes.

Material properties	**1.2738**
Density ρ [kg/m³]	7600
Heat capacity c [J/kg/K]	550
Thermal diffusivity κ ($\cdot 10^{-6}$) [m²/s]	6.699
Specific melting enthalpy q_m [kJ/kg]	209
Melting temperature T_m [K]	1759.15
Melting temperature enthalpy corrected $T_{m,q}$ [K]	2139.15
Absorptance A [-]	0.44

5. Results and Discussion

5.1. Influence of fluence and pulses per burst

The influence of the applied fluence on the melt pool depth and the roughness is investigated in this part of the work. Square fields are laser polished on the ground initial surface with two repetitions ($N = 2$). The fluence F_0 is varied from 0.100 to 0.165 J/cm² for $PpB = 14$ and from 0.065 to 0.140 J/cm² for $PpB = 20$.

The melt pool depth reveals an approximately linear dependency on the fluence used in the investigated parameter range. The greater the energy throughout a burst, the deeper the heat penetrates the bulk material. This thermal energy causes the temperature to rise above the melting point to a certain depth in the workpiece, which is eventually the measured melt pool depth.

The micro roughness, on the other hand, shows a global minimum in the range of $F_0 = 0.120$–0.140 J/cm² for $PpB = 14$

(see Fig. 1) and F_0 = 0.085–0.110 J/cm² for PpB = 20 (see Fig. 2). If the energy input is too low, it does not induce a sufficiently deep melt pool for a good micro polishing result. However, as soon as the melt pool becomes too large, the dynamics of the melt causes a roughening of the surface [16]. In addition to that, material evaporation begins, as the process surpasses the ablation threshold. For F_0 > 0.155 J/cm² at PpB = 14 and for F_0 > 0.130 J/cm² at PpB = 20 the processed surface exceeds the micro roughness of the ground initial surface, which is S_a = 0.12 µm. Good micro polishing results are achieved when the melt pool depth is about z_m = 1–2 µm for PpB = 14 and z_m = 2–3 µm for PpB = 20. The meso roughness also follows the shape of the micro roughness curve but with a global minimum at a greater fluence. It can only be successfully smoothed with PpB = 20, namely from $S_{a,meso}$ = 0.15 µm to 0.10 µm, but not with PpB = 14. The meso roughness stays unchanged in the best case of PpB = 14.

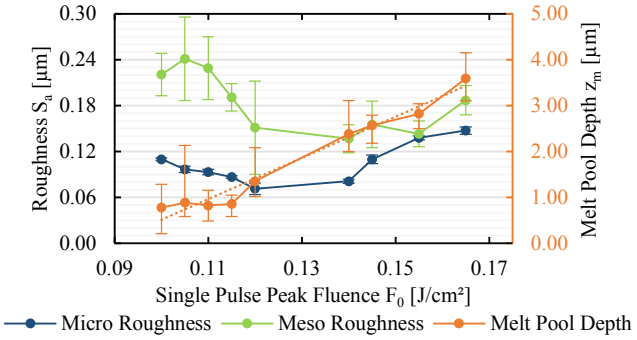

Fig. 1. The influence of the single pulse peak fluence F_0 on the micro roughness S_a (1.6 < λ < 10 µm), meso roughness $S_{a,meso}$ (10 < λ < 80 µm) and the melt pool depth z_m at PpB = 14.

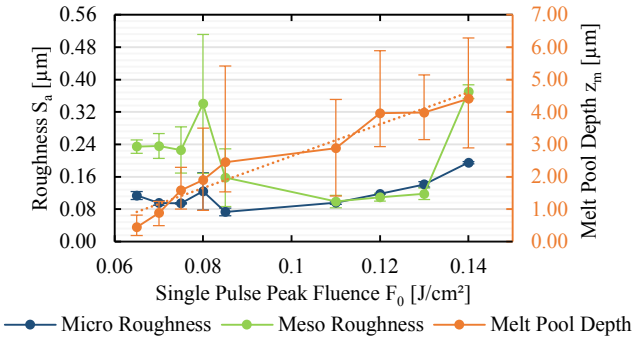

Fig. 2: The influence of the single pulse peak fluence F_0 on the micro roughness $S_{a,micro}$ (1.6 < λ < 10 µm), meso roughness $S_{a,meso}$ (10 < λ < 80 µm) and the melt pool depth z_m at PpB = 20.

Fig. 3 shows the simulated melt pool depths z_m as a function of PpB and F_0 in comparison to the real measurements. The smaller the number of pulses per burst, the higher the single pulse peak fluence needs to be to reach the melting temperature of the material. After z_m > 1 µm the melt pool depth increases approximately linearly with increasing fluence, which was also the result of the experimental analysis.

The average deviation of the simulated melt pool depth from the real depth is about 0.5 µm. The calculated melt pool depths tend to be underestimated in the simulation for small energy inputs and overestimated for large energy inputs. The reason for that might lie in the simplified material properties like the thermal diffusivity or the absorptance.

Another finding from the simulation is that the temperature on the surface does not sink below the material specific melting temperature after a start-phase of 10 applied pulses. A continuous melt pool is guided along the scan vector, as already described by BRENNER et al. [6].

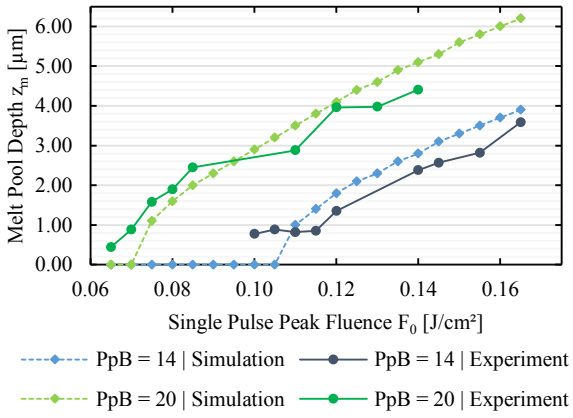

Fig. 3. Results for the induced melt pool depths z_m from the simulation model with η_{res} = 0.44.

5.2. Influence of number of repetitions

A fluence of F_0 = 0.110 J/cm² at PpB= 19 is used to investigate the influence of the number of repetitions on the micro/meso roughness and the melt pool depth. The applied numbers of repetitions are 2, 8, 32 and 128. The tests are conducted under ambient air. The results are shown in Fig. 4.

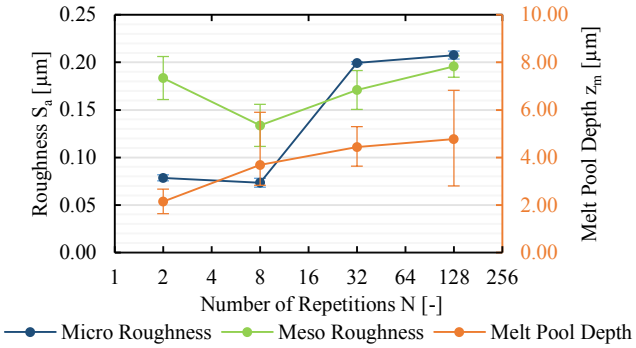

Fig. 4. The influence of the number of repetitions N on the micro roughness (1.6 < λ < 10 µm), meso roughness (10 µm < λ < 80 µm) and the melt pool depth z_m at PpB = 19, F_0 = 0.105 J/cm².

The melt pool depth z_m increases as the number of repetitions increases. Saturation can be assumed here, but not before N > 128. The increasing melt pool depth can be explained by an increasing absorption mainly due to oxidation [17,18]. At some point, the absorption is increased to such an extent that

the melt pool and thus also the melt dynamics cause a roughening of the surface (see section 5.1). A rougher surface then results in a higher absorption again [18,19].

The micro roughness does not change significantly from $N = 2$ to 8, but there is a strong increase from 8 to 32 repetitions. When applying more than $N = 32$, it seems like the micro roughness undergoes a saturation. In contrast to that, the meso roughness drops significantly from $N = 2$ to 8 which is a strong indicator that roughness components of larger spatial wavelengths need more repetitions and/or a deeper melt pool to be smoothed.

For the first time, ablation is detected during ultrashort pulse laser polishing although the single pulse fluence F_0 is below the threshold fluence F_{thr} of the material. To exclude heat accumulation through subsequent repetitions, the test for $N = 128$ is repeated, but with a delay of 5 seconds after every two repetitions. As can be seen in Fig. 5, the result remains the same.

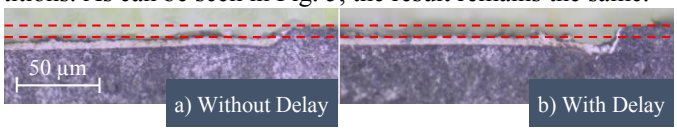

Fig. 5. Micrographs of the cross-section polish after 128 repetitions at $PpB = 19$, $F_0 = 0.105$ J/cm² (a) without a delay between the repetitions; (b) with a delay between the repetitions.

The heat accumulation during one burst causes preheating that adds energy to the incident pulses so that a lower pulse energy is needed to evaporate material. After $N = 128$ the ablation depth is $z_{abl} = 6.75$ µm, which corresponds to an average ablation depth of $z_{abl} = 0.05$ µm per repetition. In practical applications, where a low roughness is required, only a low number of repetitions would be chosen. Considering the much smaller absorption prevailing in that regime, the actual removal rate is probably much lower.

This observation disproves the assumption made for the simulation that no energy flows into the ablation during ultrashort pulse laser polishing. It is assumed that good polishing results are always accompanied by a small amount of ablation.

5.3. Structural change of the surface layer

Based on the determined melt pool depths, two parameter sets are selected for the EBSD analysis: The parameter set $F_0 = 0.10$ J/cm² at $PpB = 14$ has a relatively shallow thermal impact, while $F_0 = 0.11$ J/cm² at $PpB = 20$ induces a relatively deep melt pool. The ground initial surface is also analyzed as reference. The crystal orientation map of the specimen with inverse pole figure (IPF) coloring is shown in Fig. 6.

The microstructure of the bulk is very coarse and randomly oriented. The melting layer clearly stands out in the images with its much finer microstructure that is also randomly oriented and uninfluenced by the last scan directions. There is no obvious heat-affected zone that might be visible as change in the microstructure. The thin layer of the fine microstructure in the blank that is not laser treated probably stems from the sample preparation steps, particularly the cross grinding and the mechanical polishing that leads to rounded edges.

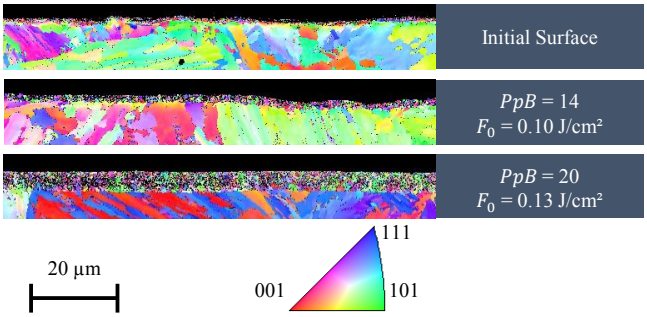

Fig. 6. IPF-images from the EBSD-Analysis.

6. Conclusion

The results of this work prove that ultrashort pulse laser polishing is particularly suitable for reducing the roughness of very fine structures due to the relatively small melt pool depth of $z_m = 1$–3 µm. It has been shown that a too large melt pool depth has negative effects on the surface quality. The simulation model predicts the melt pool depth with an average accuracy of 0.5 µm. The melt pool depth increases with increasing fluence and pulses per burst. Surprisingly, the number of repetitions also shows a positive correlation with the melt pool depth. Heat accumulation due to subsequent repetitions could be excluded as a reason. The increasing melt pool depth probably stems from an increasing absorptance due to oxidation and roughness. While the micro roughness (1.6 µm $< \lambda <$ 10 µm) remains constant from 2 to 8 repetitions, the meso roughness (10 µm $< \lambda <$ 80 µm) decreases significantly. The minimal ablation in the range of <50 nm per polishing layer has been observed for the first time but it is negligible for industrial applications. EBSD analysis has shown that the solidified melt produces a very fine-grained microstructure of random orientation in contrast to the coarse microstructure of the bulk.

For future research, USP polishing under an inert gas atmosphere should be investigated as it has demonstrated good polishing results in conventional laser polishing due to the suppression of oxidation. Another promising approach of conventional laser polishing is the application of a homogeneous intensity distribution of the focal spot (top-hat profile) to avoid local material evaporation in the center of the Gaussian beam [13].

The feasibility of laser polishing using fs-pulses has to be tested as well. In terms of surface quality and ablation efficiency the fs-laser already outperforms the ps-laser in microstructuring of metal surfaces. Therefore, a sequential process chain using fs-ablation and fs-polishing is desirable.

7. References

[1] A. Brenner, M. Zecherle, S. Verpoort, K. Schuster, C. Schnitzler, M. Kogel-Hollacher, M. Reisacher, B. Nohn, Efficient production of design textures on large-format 3D mold tools, Journal of Laser Applications 32 (2020) 12018. https://doi.org/10.2351/1.5132401.

[2] C. Nüsser, J. Kumstel, T. Kiedrowski, A. Diatlov, E. Willenborg, Process- and Material-Induced Surface Structures During Laser Polishing, Adv. Eng. Mater. 17 (2015) 268–277. https://doi.org/10.1002/adem.201400426.

[3] E. Willenborg, K. Wissenbach, N. Pirch, Verfahren zum Glätten und Polieren von Oberflächen durch Bearbeitung mit Laserstrahlung. Patent, DE 102 28 743 B4, 2002.

[4] A.M.K. Hafiz, Applicability of a Picosecond Laser for Micro-Polishing of Metallic Surfaces. Dissertation, London, Ontario, Canada, 2013.

[5] A. Pauli, Faster and Smoother Thanks to Laser Polishing, LTJ 11 (2014) 46–48. https://doi.org/10.1002/latj.201400044.

[6] A. Brenner, L. Röther, M. Osbild, J. Finger, Laser polishing using ultrashort pulse laser, in: Laser-based Micro- and Nanoprocessing XIV, San Francisco, United States, SPIE, 01.02.2020 – 06.02.2020. https://doi.org/10.1117/12.2551481

[7] K. Wissenbach, E. Willenborg, T. Kiedrowski, Verfahren zum Glätten und Polieren oder zum Strukturieren von Oberflächen mit Laserstrahlung, Patent, DE000010342750B4, 2003.

[8] B. Neuenschwander, G.F. Bucher, C. Nussbaum, B. Joss, M. Muralt, U.W. Hunziker, P. Schuetz, Processing of metals and dielectric materials with ps-laserpulses: Results, strategies, limitations and needs, in: Proceedings of the SPIE – The International Society for Optical Engineering. https://doi.org/10.1117/12.846521

[9] B. Lauer, B. Jäggi, B. Neuenschwander, Influence of the Pulse Duration onto the Material Removal Rate and Machining Quality for Different Types of Steel, Physics Procedia 56 (2014) 963–972. https://doi.org/10.1016/j.phpro.2014.08.116.

[10] G. Raciukaitis, Use of High Repetition Rate and High Power Lasers in Microfabrication: How to Keep the Efficiency High?, JLMN 4 (2009) 186–191. https://doi.org/10.2961/jlmn.2009.03.0008.

[11] Deutsches Institut für Normung e. V., Geometrische Produktspezifikation (GPS) - Oberflächenbeschaffenheit: Flächenhaft: Teil 2: Begriffe und Oberflächen-Kenngrößen (ISO 25178-2:2012); Deutsche Fassung EN ISO 25178-2:2012 17.040.30, 2020.

[12] A. Temmler, Selektives Laserpolieren von metallischen Funktions- und Designoberflächen. Zugl.: Aachen, Techn. Hochsch., Dissertation, 2013, Shaker, Aachen, 2013.

[13] C. Nüsser, Lasermikropolieren von Metallen, Dissertation, 1st ed., 2018.

[14] F. Bauer, A. Michalowski, T. Kiedrowski, S. Nolte, Heat accumulation in ultra-short pulsed scanning laser ablation of metals, Opt. Express 23 (2015) 1035–1043. https://doi.org/10.1364/OE.23.001035.

[15] B. Neuenschwander, T. Kramer, B. Lauer, B. Jaeggi, Burst mode with ps- and fs-pulses: Influence on the removal rate, surface quality, and heat accumulation, San Francisco, California, United States, SPIE, 2015, 93500U. https://doi.org/10.1117/12.2076455

[16] E. Willenborg, Polieren von Werkzeugstählen mit Laserstrahlung. Zugl.: Aachen, Techn. Hochsch., Dissertation, 2005, Shaker, Aachen, 2006.

[17] D. Bergström, The Absorption of Laser Light by Rough Metal Surfaces, Dissertation, Östersund, 2008.

[18] R. Poprawe (Ed.), Tailored Light 2: Laser Application Technology, Springer-Verlag Berlin Heidelberg, Berlin, Heidelberg, 2011.

[19] T. Wu, Y. Zhu, C. Wei, M. Zhou, L. Wang, The influence of roughness on reflectivity evolution of iron irradiated by 1064nm CW laser, Chengdu, China, SPIE, 2017, p. 1017321. https://doi.org/10.1117/12.2267822